

# Biofabrication



## PAPER

### OPEN ACCESS

RECEIVED  
11 July 2023

REVISED  
6 October 2023

ACCEPTED FOR PUBLICATION  
16 November 2023













PUBLISHED  
11 December 2023

Original content from  
this work may be used  
under the terms of the  
[Creative Commons  
Attribution 4.0 licence](#).

Any further distribution  
of this work must  
maintain attribution to  
the author(s) and the title  
of the work, journal  
citation and DOI.



## Stress-free cell aggregation by using the CEPT cocktail enhances embryoid body and organoid fitness

Seungmi Ryu<sup>1,\*</sup> , Claire Weber<sup>1</sup> , Pei-Hsuan Chu<sup>1</sup>, Ben Ernest<sup>2</sup>, Vukasin M Jovanovic<sup>1</sup> , Tao Deng<sup>1</sup>, Jaroslav Slamecka<sup>1</sup> , Hyenjong Hong<sup>1</sup>, Yogita Jethmalani<sup>1</sup> , Hannah M Baskir<sup>1</sup> , Jason Inman<sup>1</sup> , John Braisted<sup>1</sup> , Marissa B Hirst<sup>2</sup>, Anton Simeonov<sup>1</sup> , Ty C Voss<sup>1</sup> , Carlos A Tristan<sup>1</sup>  and Ilyas Singeç<sup>1,\*</sup> 

<sup>1</sup> National Center for Advancing Translational Sciences (NCATS), Stem Cell Translation Laboratory (SCTL), National Institutes of Health (NIH), Rockville, MD 20850, United States of America

<sup>2</sup> Rancho Biosciences, 16955 Via Del Campo, #200, San Diego, CA 92127, United States of America

\* Authors to whom any correspondence should be addressed.

E-mail: [seungmi.ryu@nih.gov](mailto:seungmi.ryu@nih.gov) and [ilyassingec@gmail.com](mailto:ilyassingec@gmail.com)

**Keywords:** embryoid body, cytoprotection, organoid, pluripotent stem cell, polypharmacology, iPSCs, CEPT cocktail

Supplementary material for this article is available [online](#)

### Abstract

Embryoid bodies (EBs) and self-organizing organoids derived from human pluripotent stem cells (hPSCs) recapitulate tissue development in a dish and hold great promise for disease modeling and drug development. However, current protocols are hampered by cellular stress and apoptosis during cell aggregation, resulting in variability and impaired cell differentiation. Here, we demonstrate that EBs and various organoid models (e.g., brain, gut, kidney) can be optimized by using the small molecule cocktail named CEPT (chroman 1, emricasan, polyamines, trans-ISRIB), a polypharmacological approach that ensures cytoprotection and cell survival. Application of CEPT for just 24 h during cell aggregation has long-lasting consequences affecting morphogenesis, gene expression, cellular differentiation, and organoid function. Various qualification methods confirmed that CEPT treatment enhanced experimental reproducibility and consistently improved EB and organoid fitness as compared to the widely used ROCK inhibitor Y-27632. Collectively, we discovered that stress-free cell aggregation and superior cell survival in the presence of CEPT are critical quality control determinants that establish a robust foundation for bioengineering complex tissue and organ models.

## 1. Introduction

Controlling cell fate, differentiation, and maturation of human tissues *in vitro* are among the most formidable challenges in biomedical research. Self-renewing human pluripotent stem cells (hPSCs), such as induced pluripotent stem cells (iPSCs), serve as an inexhaustible source of human cells and tissues and provide invaluable insights into normal development and human diseases [1–5]. *In vitro*-generated organoids exhibit a remarkable potential for self-organization and recapitulate important aspects of organogenesis. Depending on the tissue of interest, different protocols have been developed to control lineage commitment and cell fate specification by modulating specific cell signaling pathways and providing the appropriate

physicochemical environment for differentiating cells [6]. Recent cell culture advances allow for extended culture of organoids for periods ranging from several months to years [5, 7, 8].

Stem cells are generally grown on cell culture plates coated with a substrate (e.g., laminin, vitronectin) and generation of three-dimensional (3D) cultures from these cells requires detachment and single-cell dissociation. Preparing the cellular material, plating cells into ultra-low attachment plates, and aggregating cells into 3D structures are associated with marked cellular stress and cell death by apoptosis and anoikis [9]. Dissociated hPSCs respond with hyperactivation of the ROCK pathway leading to cell contractions and cell death [3, 5, 10–13]. To deal with poor cell survival, one can compensate by plating a higher number of cells or by using reagents

that partially improve cell survival, as demonstrated with the application of 10–50  $\mu\text{M}$  ROCK pathway inhibitor Y-27632 [3, 5, 11–13]. However, suboptimal approaches can contribute to product variation and non-standardized organoid models pose challenges for reproducibility and experimental rigor in disease modeling and drug discovery [14].

In direct comparison to Y-27632, the four-part small molecule cocktail (CEPT) has been shown to strongly improve viability of hPSCs during routine monolayer cell passaging, single-cell cloning, cryopreservation/thawing, gene editing, embryoid body (EB), and cerebral organoid formation [9]. In the present study, we expanded on this work and provide a detailed and systematic analysis of the beneficial effects of CEPT for stress-free cell aggregation as a critical step for initiating 3D cell culture models. The beneficial effects of CEPT were applicable to EBs, different brain organoids (cortical and cerebral) as well as intestinal and kidney organoids. Optimal cell aggregation by CEPT during the first 24 h strongly impacted the biology of self-organizing EBs and organoids including overall size, architecture, differentiation, maturation, and function. Hence, the new data presented in this study should help establish an urgently needed chemical platform for standardization and reproducibility of 3D culture models to minimize cell culture artifacts.

## 2. Experimental section

More detailed descriptions of experimental procedures are provided in supplemental information.

### 2.1. Chemical compounds

ROCK inhibitor Y-27632 (Tocris, 10  $\mu\text{M}$ , unless otherwise stated) and CEPT cocktail components (chroman 1, MedChemExpress, 50 nM; emricasan, Selleckchem 5  $\mu\text{M}$ ; polyamine supplement, Sigma Aldrich, 1:1000; trans-ISRIB, Tocris, 0.7  $\mu\text{M}$ ) were prepared following the manufacturer's recommendations.

### 2.2. Cell culture and organoid formation

All hESC (WA09) and hiPSC (LiPSC-GRI.1, GM23279, and GM25256) lines were maintained under feeder-free conditions in mTeSR medium (STEMCELL Technologies) and VTN-N-coated (Thermo Fisher Scientific) plates as described in the supplemental information. Cerebral, intestinal, and kidney organoids were generated using commercial kits (STEMCELL Technologies) or a previously published protocol for cortical organoids [5]. For high-content 3D imaging, cerebral organoids were generated at various starting cell numbers (1500–7500 cells per organoid). A customized image analysis script was used for the automated measurement of sphere features. Details on the functional analyses of organoids are described in the supplemental information.

### 2.3. EB viability analysis

The CellTiter-Glo 3D assay (Promega) was used to quantify cell viability and performed following the instructions of the manufacturer. EB size was measured using the Celigo Imaging Cytometer (Nexcelom Biosciences). Live and dead cells were determined using a two-color fluorescence live/dead assay kit (Thermo Fisher Scientific, 1:2000).

### 2.4. Western blot

Western blot analyses were performed using the Wes automated western blotting system (Protein Simple) following the manufacturer's instructions.

### 2.5. Gene expression analysis

For RASL-seq analysis, hESCs (WA09) were dissociated and cultured at a density of 20,000 cells per well in 96-well ULA round-bottom plates (Corning) in E6 medium (Thermo Fisher Scientific) for 7 d. For bulk RNA-sequencing analysis, three organoids were pooled to prepare a sample (three samples per group). RNA was extracted using the RNeasy Mini Kit (Qiagen). For reproducibility studies, RNA was extracted from single organoids. Extracted RNA was prepped for RNA-Seq libraries with the TruSeq Stranded mRNA Library Prep Kit (Illumina). For single-cell RNA sequencing analysis, organoids (day 72) were dissociated into single cells using the Embryoid Body Dissociation kit (Miltenyi Biotec) and gentle MACS Dissociator (Miltenyi Biotec) following the manufacturer's protocol. The strained cell suspension was loaded on a Chromium Controller (10X Genomics) to generate single-cell gel bead-in-emulsions (GEM) and barcoding. The library was sequenced on an Illumina NextSeq 550. More details on library preparation and bioinformatic analysis are described in the supplemental information.

## 3. Results

### 3.1. Optimizing EB formation using CEPT

EB formation is a widely used assay to measure the pluripotent differentiation potential of hPSCs [15, 16]. Differentiating EBs emulate the gastrulation process of the developing embryo and generate the three primary germ layers (ectoderm, mesoderm, endoderm). EB formation is often also the first step when generating various organoid models from hPSCs [1, 17–20]. For instance, a kit-based brain organoid protocol (STEMCELL Technologies) uses EB formation as the first step (figure 1(A)). We first compared 10  $\mu\text{M}$  Y-27632 to CEPT (50 nM chroman 1, 5  $\mu\text{M}$  emricasan, 1X polyamine supplement, and 0.7  $\mu\text{M}$  trans-ISRIB) or its two-component combination consisting of chroman 1 and emricasan (CE). The optimal concentrations of each component of the CEPT cocktail were previously established based on full dose-response curves [9]. When EBs were

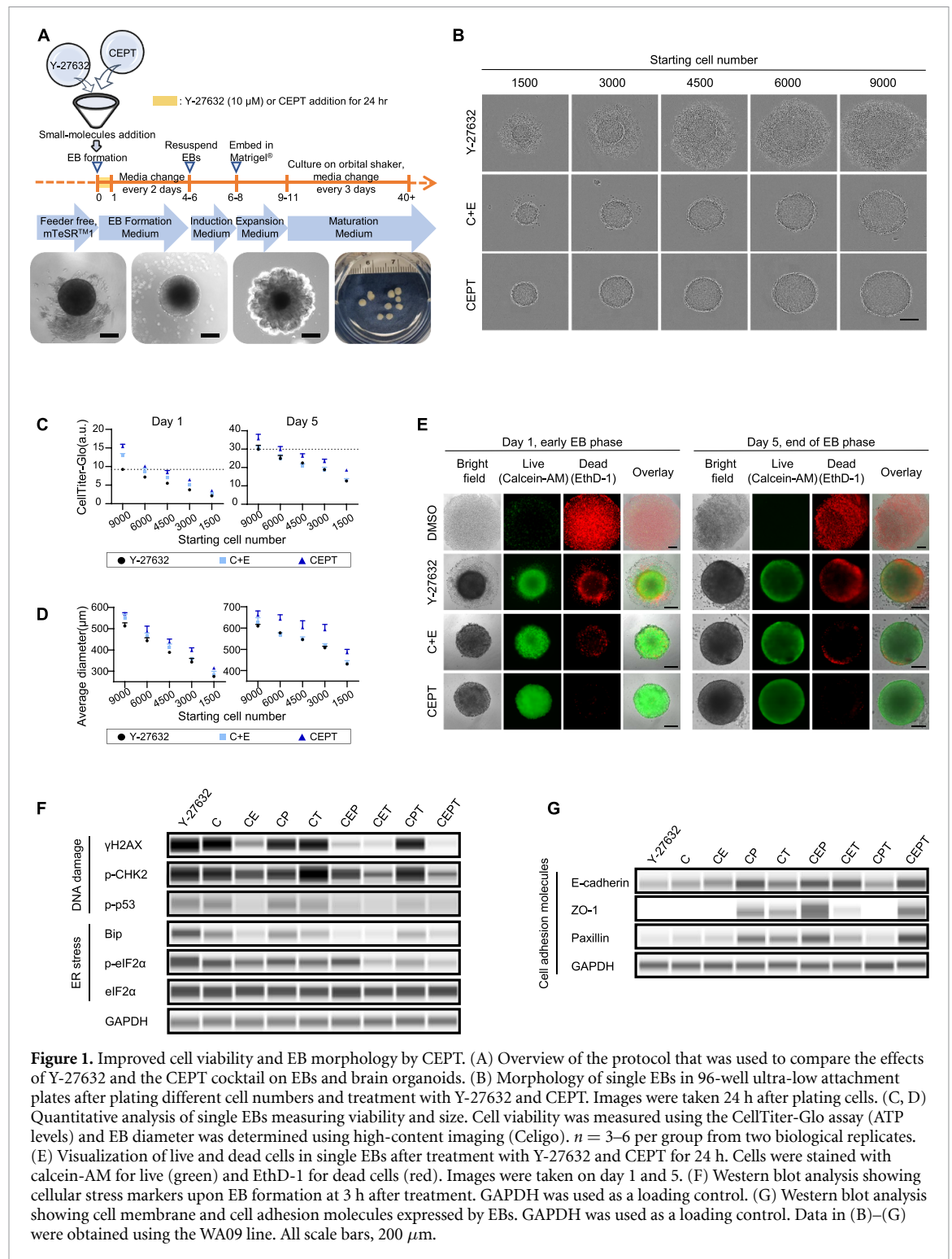


**Figure 1.** Improved cell viability and EB morphology by CEPT. (A) Overview of the protocol that was used to compare the effects of Y-27632 and the CEPT cocktail on EBs and brain organoids. (B) Morphology of single EBs in 96-well ultra-low attachment plates after plating different cell numbers and treatment with Y-27632 and CEPT. Images were taken 24 h after plating cells. (C, D) Quantitative analysis of single EBs measuring viability and size. Cell viability was measured using the CellTiter-Glo assay (ATP levels) and EB diameter was determined using high-content imaging (Celigo).  $n = 3-6$  per group from two biological replicates. (E) Visualization of live and dead cells in single EBs after treatment with Y-27632 and CEPT for 24 h. Cells were stained with calcein-AM for live (green) and EthD-1 for dead cells (red). Images were taken on day 1 and 5. (F) Western blot analysis showing cellular stress markers upon EB formation at 3 h after treatment. GAPDH was used as a loading control. (G) Western blot analysis showing cell membrane and cell adhesion molecules expressed by EBs. GAPDH was used as a loading control. Data in (B)–(G) were obtained using the WA09 line. All scale bars, 200  $\mu\text{m}$ .

generated under these three conditions and tested after 24 h, the CEPT cocktail was superior to Y-27632 and CE. Indeed, when plating different cell numbers, CEPT consistently yielded improved cell survival (CellTiter-Glo assay) and larger EBs as measured at day 1 and 5 (figures 1(B)–(D)). In direct comparison and based on plating the same cell numbers, the diameter of EBs was consistently larger after CEPT treatment versus Y-27632 (figure 1(D)). Interestingly,

to generate EBs of comparable size a higher number of cells (9000) was required for Y-27632 versus CEPT (6000 cells) (figure 1(D)). Improved cell survival and EB formation due to CEPT were confirmed in hESCs (WA09) and three different hiPSC lines (LiPSC-GR1.1, GM23279, GM25256) (supplementary figures 1(A) and (B)). Moreover, improved EB formation and morphology with CEPT was confirmed using live-cell microscopy (day 1 and 5) and

application of dyes that label live cells (calcein-AM) and dead cells (EthD-1) (figure 1(E)); quantification of cell viability is shown for 9000 cells in figure 1(C)). Confocal microscopy underscored the importance of using CEPT for optimal cell aggregation during the first 24 h (supplementary figure 1(C)). In contrast, Y-27632 treatment resulted in dead cells that were not only attached to the EB surface but also found to be enclosed within EBs as revealed by reconstructing confocal sections (Z-stack). These observations suggest that in the absence of CEPT, dead cells and cellular debris are trapped inside the EBs during cell aggregation.

Next, we asked how Y-27632, CEPT and its individual components may affect markers of DNA damage, endoplasmic reticulum (ER) stress, and the expression of cell membrane proteins. Without the use of any ROCK inhibitors (Y-27632 or chroman 1 (C)), dissociated hPSCs underwent massive cell death and failed to form EBs in chemically defined E6 medium (figure 1(E), DMSO). Western blot experiments (figure 1(F) and supplementary figure 3(A)) showed synergy between chroman 1 (C) and emricasan (E) in preventing DNA damage and ER stress, which was in contrast to chroman 1 combined with either trans-ISRIB (T) and polyamines (P). Furthermore, the addition of polyamines showed a specific beneficial effect on molecules involved in cell adhesion and cell–cell contact (E-cadherin, ZO-1, paxillin) during EB formation (figure 1(G) and supplementary figure 3(A)). Overall, our data demonstrate that CEPT treatment reduces cellular stress and DNA damage while promoting cell viability and expression of cell membrane proteins (figures 1(F) and (G)). To further strengthen these findings, we systematically investigated how EB cell viability is affected by different combinations of the four components of CEPT at 24 h post-treatment. Consistent with the Western blot data (figure 1(F) and supplementary figure 3(A)), cell viability experiments (Cell-Titer Glo) showed that treatment with CE, CT, or CET significantly improved EB cell viability (supplementary figure 2(A), shown in C vs CE, C vs CT, C vs CET). Additionally, P only improved cell viability when used in combination with C, E, and T as CEPT (supplementary figure 2(A), shown in C vs CP and CET vs CEPT). Hence, the synergistic activity of all four CEPT components is necessary to achieve optimal cell survival and EB formation, while avoiding cell stress and DNA damage.

### 3.2. CEPT enhances EB formation for high-throughput applications

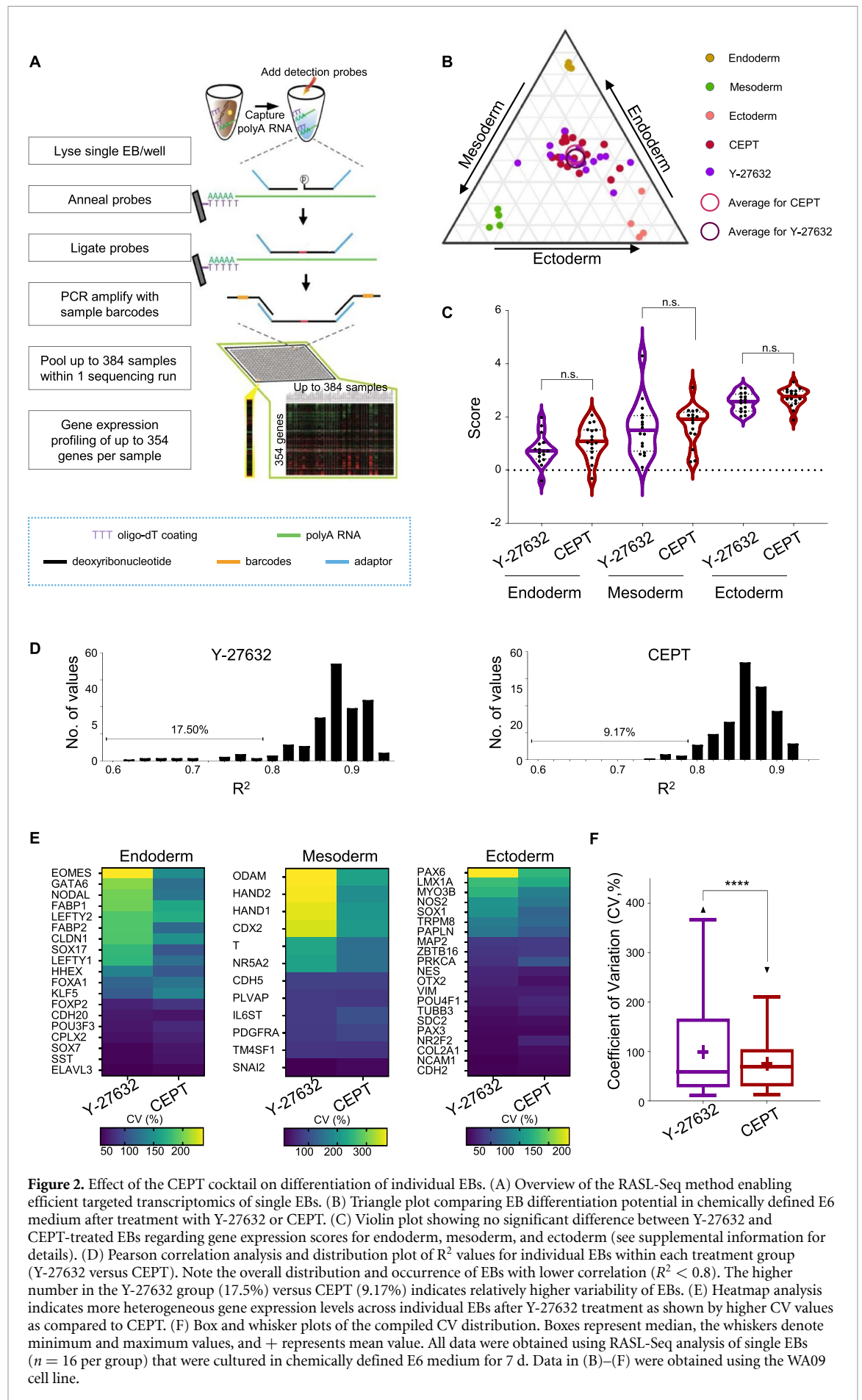
To characterize the outcome of improved viability and stress-free EB formation, we focused on analyzing single EBs. Profiling gene expression from single EBs is technically challenging since the RNA yield is typically very low and therefore difficult to implement

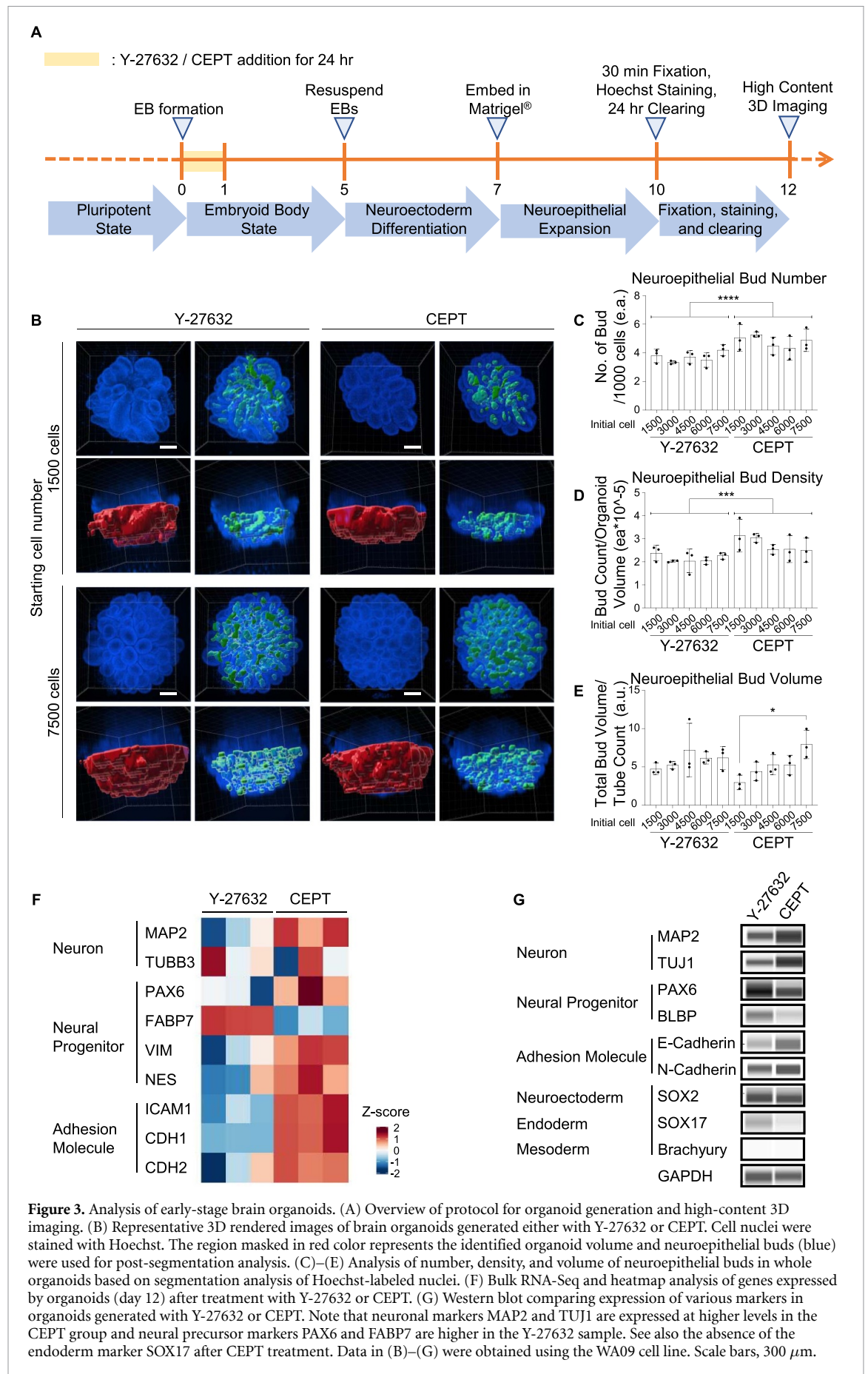
for high-throughput experiments. To overcome this challenge, we established RNA-mediated oligonucleotide Annealing, Selection, and Ligation with next-generation sequencing (RASL-Seq) for analysis of single EBs in 384-well plates (figure 2(A)). This targeted transcriptomic approach allows direct and reproducible analysis of small RNA amounts as low as 10 ng [21]. RASL-Seq is an efficient method for large-scale transcriptomic analysis of single EBs, which enables direct analysis of RNA levels in EB lysates without the need for cDNA generation and can therefore be performed in a fully automated fashion (figure 2(A)). To this end, we designed a probe set focusing on lineage-specific genes (19 genes for endoderm, 12 genes for mesoderm, 21 genes for ectoderm; genes listed in figure 2(E)). Single EBs (20,000 cells/well) generated in the presence of Y-27632 or CEPT during the first 24 h, cultured in E6 medium for 7 d, and then processed for RASL-Seq analysis (figure 2(A)). Gene expression profiling of single EBs ( $n = 16$  per group) showed multi-lineage differentiation in both conditions (figures 2(B) and (C)). However, when analyzing the biological variability across individual EBs by measuring the coefficient of determination ( $R^2$ ), we observed considerable differences (figure 2(D)).

Indeed, the coefficient was higher after CEPT treatment versus Y-27632 (total of 120 paired values comparing 16 individual EBs within the same treatment group). While 17.5% of the paired comparisons among EBs generated with Y-27632 showed an  $R^2$  value lower than 0.8, the value for CEPT-treated EBs was only 9.17%. Variation in expression of each gene across individual EBs, indicated as a coefficient of variation (CV), was higher in the Y-27632 treatment versus CEPT (figures 2(E) and (F)) for important lineage-determining transcription factors (e.g., SOX17 for endoderm, HAND2 for mesoderm, and PAX6 for ectoderm). Collectively, these findings suggest that CEPT reduced variability and promoted standardization of EBs, a widely used *in vitro* model to study pluripotency and generate organoids of different developmental lineages.

### 3.3. Optimizing brain organoids by using CEPT

We next asked whether CEPT treatment might affect the morphogenesis of brain organoids. To generate brain organoids, we used a kit-based method (figures 1(A) and 3(A)) that starts with EB formation followed by differentiation into prominent neuroepithelial buds [18, 22]. These neuroepithelial buds represent neural tube-like structures and recapitulate some aspects of early brain development. We compared organoids generated with Y-27632 or CEPT added for 24 h during EB formation. By the end of the neuroepithelial expansion phase on day 10 (figure 3(A)), whole organoids were fixed and subjected to optical clearing using a published protocol





[23]. High-content confocal microscopy was used to analyze individual organoids, which were stained with the nuclear marker Hoechst to visualize all cells (figure 3(B)). Automated analysis based on image segmentation and 3D rendering was performed to detect and quantify the number of neural buds generated per 1000 cells (figure 3(C)), the density of buds per organoid volume (figure 3(D)), and bud size (figure 3(E)). This systematic analysis revealed that CEPT-generated organoids contained more neuroepithelial buds as compared to Y-27632. We also noted that the size of the neuroepithelial buds correlated with the number of seeded cells in the CEPT treatment group ( $R^2 = 0.8848$ ), while such correlation was not found for organoids generated using Y-27632 ( $R^2 = 0.4178$ ) (figure 3(E)).

Next, we performed RNA sequencing (RNA-Seq) to examine early-stage organoid differentiation (day 12). Heatmap analysis of cell-type-specific genes (e.g. neural progenitors and neurons) and cell adhesion molecules involved in neuronal differentiation [24] showed marked differences between organoids generated with Y-27632 or CEPT (figure 3(F)). These findings suggested that CEPT-generated organoids were relatively more differentiated and showed higher expression of neuronal-associated genes and cell adhesion molecules at day 12. To further corroborate these observations, these early-stage organoids (day 12) were subjected to Western blot analysis.

CEPT-treated organoids expressed higher levels of neuronal marker MAP2 and different cell adhesion molecules (ICAM3, CDH1, CDH2), along with lower levels of the neural precursor markers PAX6 and FABP7 (also known as BLBP) (figure 3(G) and supplementary figure 3(B)). While we observed variations in TUBB3 gene transcripts among replicates, we did not observe a significant difference between Y-27632 vs CEPT (figure 3(F)).

However, Western blot data showed higher expression of neuronal marker TUJ1, the antibody against TUBB3, in organoids generated with CEPT versus Y-27632 (figure 3(G) and supplementary figure 3(C)). SOX2 expression was at similar levels in both groups and the endoderm marker SOX17 was expressed in the Y-27632 group, while it was absent in CEPT-generated organoids. The mesoderm marker brachyury was not detected in either group. Together, we conclude that under these culture conditions CEPT was superior in promoting neural lineage entry and neuronal differentiation as compared to Y-27632.

Next, we investigated how the different components of the CEPT cocktail affect neuronal differentiation of cerebral organoids. Expression of neuronal marker TUJ1 (beta-III tubulin) was analyzed via Western blot analysis of day-12 cerebral organoids (supplementary figure 2(B)). The data demonstrated that treatment of cerebral organoids with CE or

CT significantly improved cell viability but did not have a significant effect on organoid differentiation. However, treatment with CEP or CEPT which have been shown to enhance cell adhesion (figure 1(G)) also enhanced cerebral organoid differentiation as shown by higher expression of TUJ1 (supplementary figure 2(B)). This is consistent with a previous report also suggesting the importance of cell-cell contact when comparing 2D and 3D cultures [24]. Our data show that polyamines play important roles in cell adhesion/cell aggregation and improve neuronal differentiation of cerebral organoids.

### 3.4. CEPT treatment improves organoid architecture and *in vivo*-like differentiation

To investigate how early exposure to CEPT or Y-27632 may influence organoid biology at later stages, we cultured cerebral organoids for two months and performed several comparisons using different methods. Hematoxylin-eosin (H&E) staining showed the presence of more well-developed neural rosette-like structures in CEPT-treated organoids as compared to Y-27632 (figure 4(A) and supplementary figure 4(A)). These neural tube-like structures, which were generated more robustly with CEPT versus Y-27632, expressed the forebrain and neural precursor markers FOXG1 and SOX2 (figures 4(B) and (C)). As expected, neural tube-like structures were surrounded by neuronal cells expressing MAP2. Western blot analysis confirmed higher protein levels of markers expressed by neural progenitors (FOXG1, EN2, TBR2, and SOX2), neuroblasts (DCX), and more mature neurons (NeuN, NF200, MAP2) (figure 4(D) and supplementary figure 3(D)).

Next, we performed bulk RNA-Seq analysis of organoids that were cultured for 2 months after 24 h treatment with Y-27632 or CEPT. We compared the whole transcriptomes of these organoids to samples of the developing human cortex (8–9 weeks post-conception; Allen Brain Atlas) [26]. Indeed, this unbiased analysis using Spearman correlation revealed that the overall molecular signature of CEPT-generated organoids was more similar to early human brain tissue in contrast to Y-27632-generated organoids (figure 4(E)).

Furthermore, we asked if CEPT may have beneficial effects on inter-organoid reproducibility and compared the transcriptomes of single organoids, which were generated from three different iPSC lines. Individual organoids (day 36) generated in parallel using Y-27632 or CEPT were processed for RNA-Seq analysis. Again, we applied coefficient of determination ( $R^2$ ) analysis to measure similarity across single cerebral organoids generated from the same iPSC line. We found substantial organoid-to-organoid variability after Y-27632 treatment as indicated by the low value in the correlation plot (figure 4(F)) and higher distribution of the average

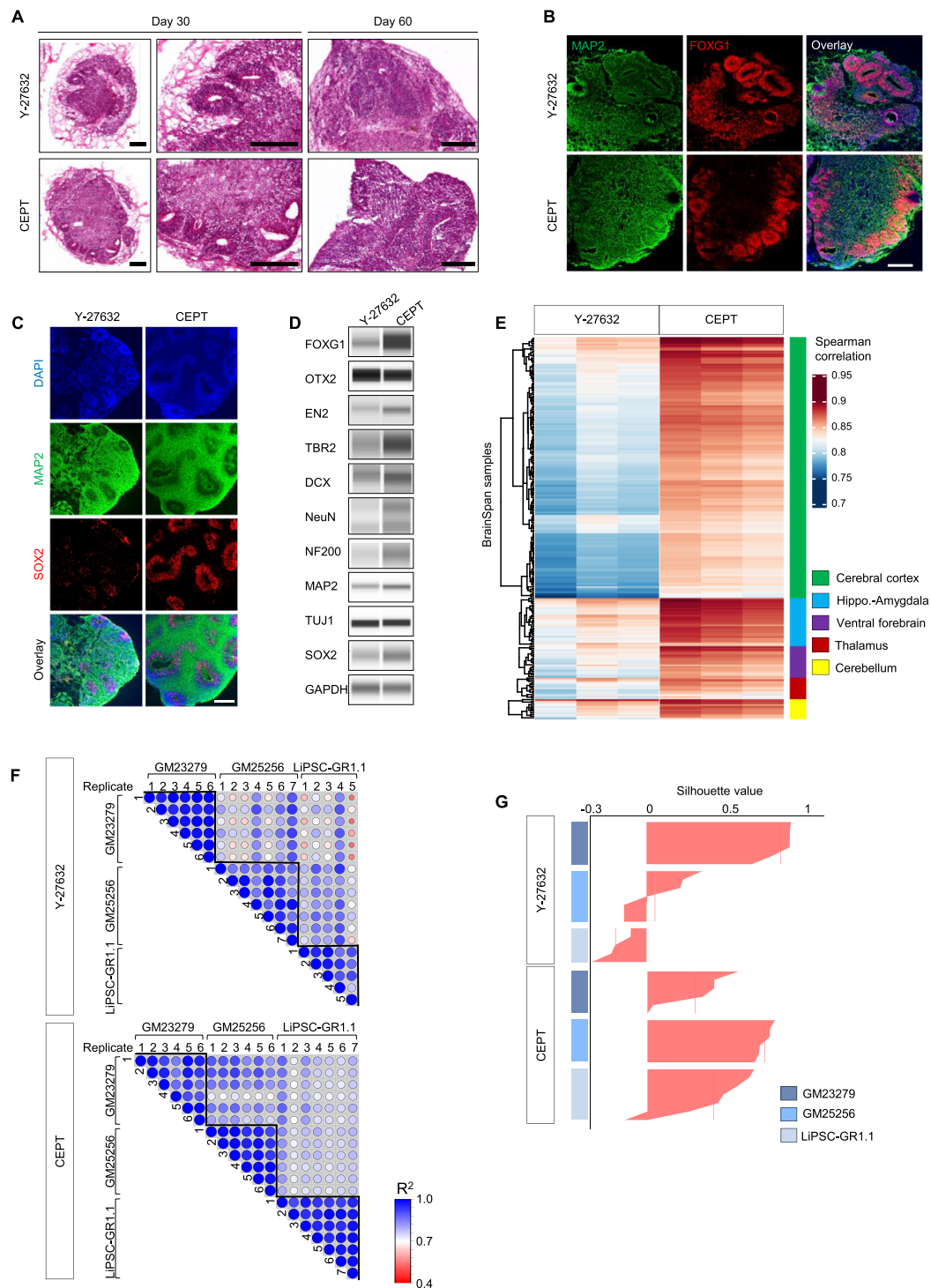


**Figure 4.** Neural architecture, comparison to brain tissue, and organoid reproducibility. (A) H&E staining of representative organoids at day 30 and day 60 derived with either Y-27632 or CEPT treatment. (B) Immunostaining of cryosectioned organoids at day 30 for forebrain marker FOXG1 and neuronal marker MAP2. Note the improved formation of neural tube-like regions after CEPT treatment. (C) Immunostaining of MAP2-labeled neurons surrounding neural tube-like structures expressing SOX2 (day 60). Note that organoid anatomy is more consistent in the CEPT-generated example. (D) Western blot analysis of cell type- and brain-region-specific markers show differences between both groups (day 36). (E) Heatmap analysis (bulk RNA-Seq) and Spearman correlation coefficients reveal differences between organoids generated with Y-27632 and CEPT (day 60) and indicate similarity to the human cortex (Allen BrainSpan Atlas). The raw data set was previously published [9], where it was compared to a large transcriptome collection of human cells and tissues in the ARCHS4 database [25]. (F) Pearson correlogram based on whole mRNA transcriptomes of individual organoids generated within the same and across different hiPSC lines at day 36.  $R^2$  values were computed with 95% confidence intervals. Deeper color represents a higher correlation ( $R^2$ ). (G) Silhouette plot based on transcriptomic analysis of individual organoids. Each bar represents single organoids derived from three cell lines. The silhouette value represents similarity within each cell line compared to the next most similar cell lines. Positive values indicate that the organoid is closer to other organoids within its cluster. The vertical line indicates the average silhouette value of each cluster. CEPT-generated organoids showed a closer average silhouette value compared to Y-27632 generated organoids. Data in (A)–(E) were obtained using WA09. Scale bars, (A) 300  $\mu\text{m}$ , (B) 300  $\mu\text{m}$ , (C) 200  $\mu\text{m}$ .



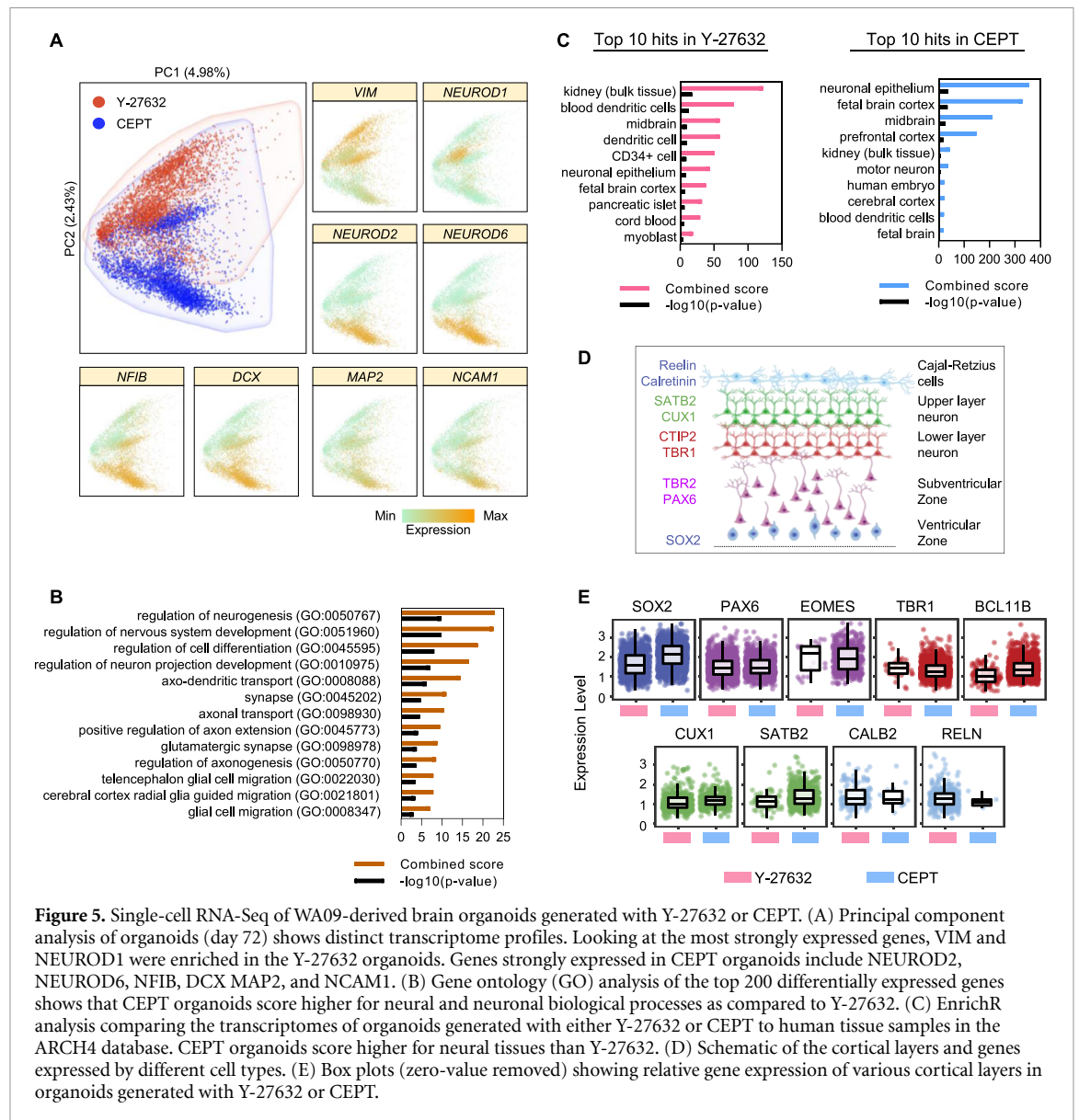


**Figure 5.** Single-cell RNA-Seq of WA09-derived brain organoids generated with Y-27632 or CEPT. (A) Principal component analysis of organoids (day 72) shows distinct transcriptome profiles. Looking at the most strongly expressed genes, VIM and NEUROD1 were enriched in the Y-27632 organoids. Genes strongly expressed in CEPT organoids include NEUROD2, NEUROD6, NFIB, DCX, MAP2, and NCAM1. (B) Gene ontology (GO) analysis of the top 200 differentially expressed genes shows that CEPT organoids score higher for neural and neuronal biological processes as compared to Y-27632. (C) EnrichR analysis comparing the transcriptomes of organoids generated with either Y-27632 or CEPT to human tissue samples in the ARCH4 database. CEPT organoids score higher for neural tissues than Y-27632. (D) Schematic of the cortical layers and genes expressed by different cell types. (E) Box plots (zero-value removed) showing relative gene expression of various cortical layers in organoids generated with Y-27632 or CEPT.

silhouette value in the silhouette plot (figure 4(G)). In contrast, CEPT-generated individual organoids displayed overall higher  $R^2$  values, indicating a higher degree of similarity. As shown in the silhouette plot, the comparison across cell lines also confirmed that CEPT reduced organoid-to-organoid variability (figures 4(F) and (G)).

### 3.5. Improved neuronal differentiation at single-cell resolution

Next, we performed single-cell RNA-Seq (10X Genomics Chromium) for organoids generated with CEPT or Y-27632. We analyzed the transcriptomes of 8,952 cells (4,280 cells for the Y-27632 group; 4672 cells for the CEPT group). Dimensionality reduction by principal component analysis showed distinct global expression profiles for each group (figure 5(A)). Top differentially expressed genes included VIM, NEUROD1, NEUROD2, NEUROD6, NFIB, DCX, MAP2, and NCAM1 (figure 5(A)).

Gene Ontology analysis based on the top 200 differentially expressed genes revealed that CEPT-generated organoids scored higher than Y-27632 organoids for neural-specific categories, including regulation of neurogenesis, neural development, axo-dendritic transport, glutamatergic synapse, and others (figure 5(B)). We performed additional gene enrichment analysis using the ARCHS4 database [25], which allows unbiased comparison to a collection of 84,863 human samples. Again, when the top-200 differentially expressed genes comparing Y-27632 vs CEPT organoids were submitted, the top-hit categories indicated improved neural differentiation in CEPT organoids, whereas organoids generated using Y-27632 scored highest in non-neural categories such as ‘kidney’ and ‘blood dendritic cells’ (figure 5(C)).

During brain development, the cortical layers are formed by neuroblasts that migrate in an inside-out pattern from the subventricular zone toward the outer layers and the pial surface, whereby

later-born neurons migrate through earlier-formed cortical layers [27]. We used immunohistochemistry to evaluate proper cortical layer formation (marked by expression of DCX, TBR1, TBR2, SATB2, and CTIP2) (supplementary figure 4(B)) in CEPT-versus Y-27632-generated organoids (day 60). In addition, single-cell RNA-Seq was performed for cell type-specific genes representing different cortical layers (figure 5(D)). Direct comparison of organoids revealed that CEPT treatment resulted in overall improved cortical development as indicated by higher and more consistent expression of various genes representing neural progenitors (SOX2, PAX6, EOMES/TBR2), as well as lower (TBR1, BCL11B/CTIP2) and upper layer neurons (CUX1, SATB2) (figure 5(E)).

Interestingly, only CALB2 and RELN, markers of Cajal–Retzius cells, were more abundant in the Y-27632 group. Given the transient role of Cajal–Retzius cells, this may indicate that CEPT organoids were relatively more mature. In conclusion, CEPT treatment during the first 24 h of cell aggregation had long-lasting consequences, improved neuronal differentiation, and the difference to Y-27632 treatment was detectable even after culturing organoids for over 2 months.

### 3.6. Single-cell analysis confirms the superiority of CEPT-generated organoids

To characterize the cellular diversity of cerebral organoids generated with CEPT or Y-27632, the gene expression of single cells was analyzed by unsupervised clustering and visualized by two-dimensional t-distributed stochastic neighbor embedding (tSNE) plot (figure 6(A)). t-SNE dimensionality reduction revealed seven distinct clusters where each cluster showed high differential gene expression, categorizing cell populations from CEPT organoids into three clusters and Y-27632 into four clusters. Unbiased cell population identification was performed based on a comparison of the expressed transcriptomes with a curated list of genes (supplementary table 2) for neural progenitors, radial glia, cortical neuron, and upper and lower cortical neurons based on a previous report [28]. The data demonstrated that CEPT clusters (clusters 1–3) showed higher enrichment for molecular signatures representing cell types of the developing cortex as compared to the Y-27632 clusters (clusters 4–7) (figure 6(A)). Gene set enrichment analysis based on the top 100 differentially expressed genes in each cluster showed significantly enriched biological pathways of neuronal development in each cluster except for cluster 3 in CEPT and cluster 7 in Y-27632 (figures 6(B) and (C), supplementary table 3 for full list of genes in figure 6(B)). While only a small fraction of cells in CEPT-generated organoids were non-neural (cluster 3), the non-neural cluster was larger in organoids generated by using Y-27632 (cluster 7). Moreover, CEPT-generated organoids showed

higher expression of several genes involved in neuronal function (SLC17A17, GRIN2B, KCNJ6, NR4A2, GABBR1, GABBR2) (figure 6(D)). The developmental expression profile of AMPA ( $\alpha$ -amino-3-hydroxy-5-methyl-4-isoxazolepropionic acid) and NMDA (*N*-methyl-D-aspartate)-type glutamate receptors, which are ligand-gated ion channels composed of specific tetrameric subunits, can indicate the level of neuronal maturation [29, 30]. We found that CEPT-treated cerebral organoids (day 60) expressed higher levels of the functionally critical AMPA receptor subunit GRIA2 (GluR2) and the critical NMDA subunit GRIN1 (GluN1) (supplementary figure 5(A)) [29, 30]. Furthermore, we found that the epigenetic regulator TET3 was expressed at higher levels after CEPT treatment (2-fold upregulated in CEPT versus Y-27632) [31]. Accordingly, neural-specific target genes of TET3 and gene ontology analysis indicated improved neuronal differentiation and maturation after CEPT treatment (supplementary figures 5(B) and (C)) [32]. Finally, cell stress markers were found to be significantly higher in neuronal clusters derived with Y-27632 as compared to CEPT. We performed Gene Ontology enrichment analysis using a curated list for cell stress-related biological pathways (supplementary table 4) based on genes that were differentially expressed in organoids generated with Y-27632 or CEPT. ER stress response was statistically higher in Y-27632 as compared to CEPT-generated organoids, with the lowest expression of cell stress-related markers found in CEPT-generated neuronal clusters (figure 6(E), supplementary figures 5(D) and (E)). Identifying these marked differences is important, thereby providing a plausible explanation and strategy to overcome cellular stress and impaired cell differentiation in cortical organoids as reported by others [33].

### 3.7. CEPT improves other neural and non-neural organoid models

To evaluate whether CEPT might be universally beneficial, we tested another brain organoid protocol [5] and two commercially available kit-based methods (STEMCELL Technologies) that generate intestinal and kidney organoids [34, 35]. First, we generated cortical organoids using 20  $\mu$ M Y-27632 [5] or CEPT (supplementary figure 6(A)). Organoids of both treatment groups were cultured until day 35 and then processed for immunohistochemical analysis. CEPT-generated organoids showed improved anatomical organization with prominent neural tube-like structures expressing PAX6 surrounded by neuronal cells expressing MAP2. In contrast, organoids generated by using Y-27632 were more variable histologically (supplementary figure 6(B)).

Next, we generated intestinal organoids from two hPSC lines (WA09 and LiPSC-GR1.1) treated with Y-27632 following the manufacturer instructions (STEMCELL Technologies) or treated with CEPT

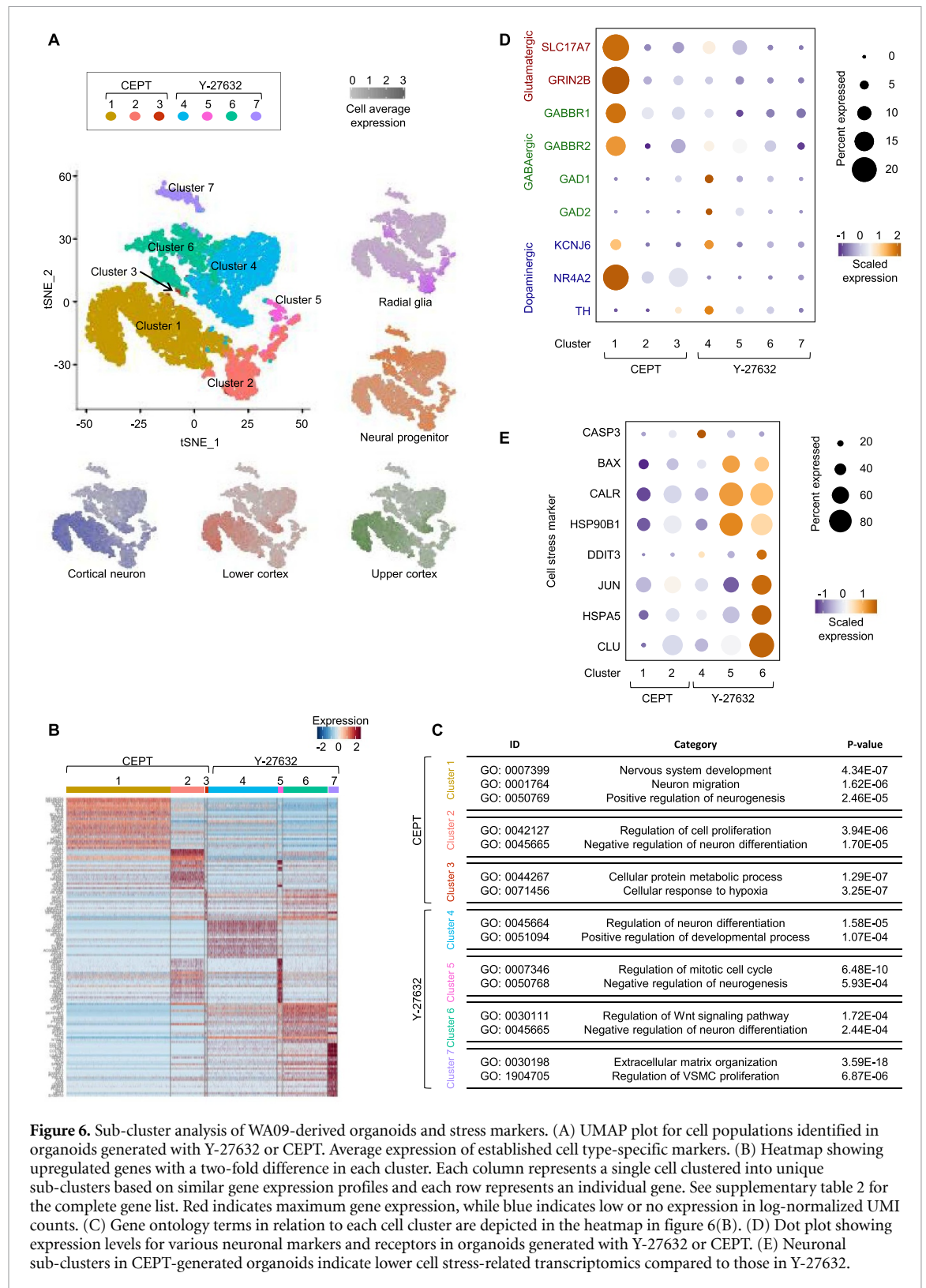
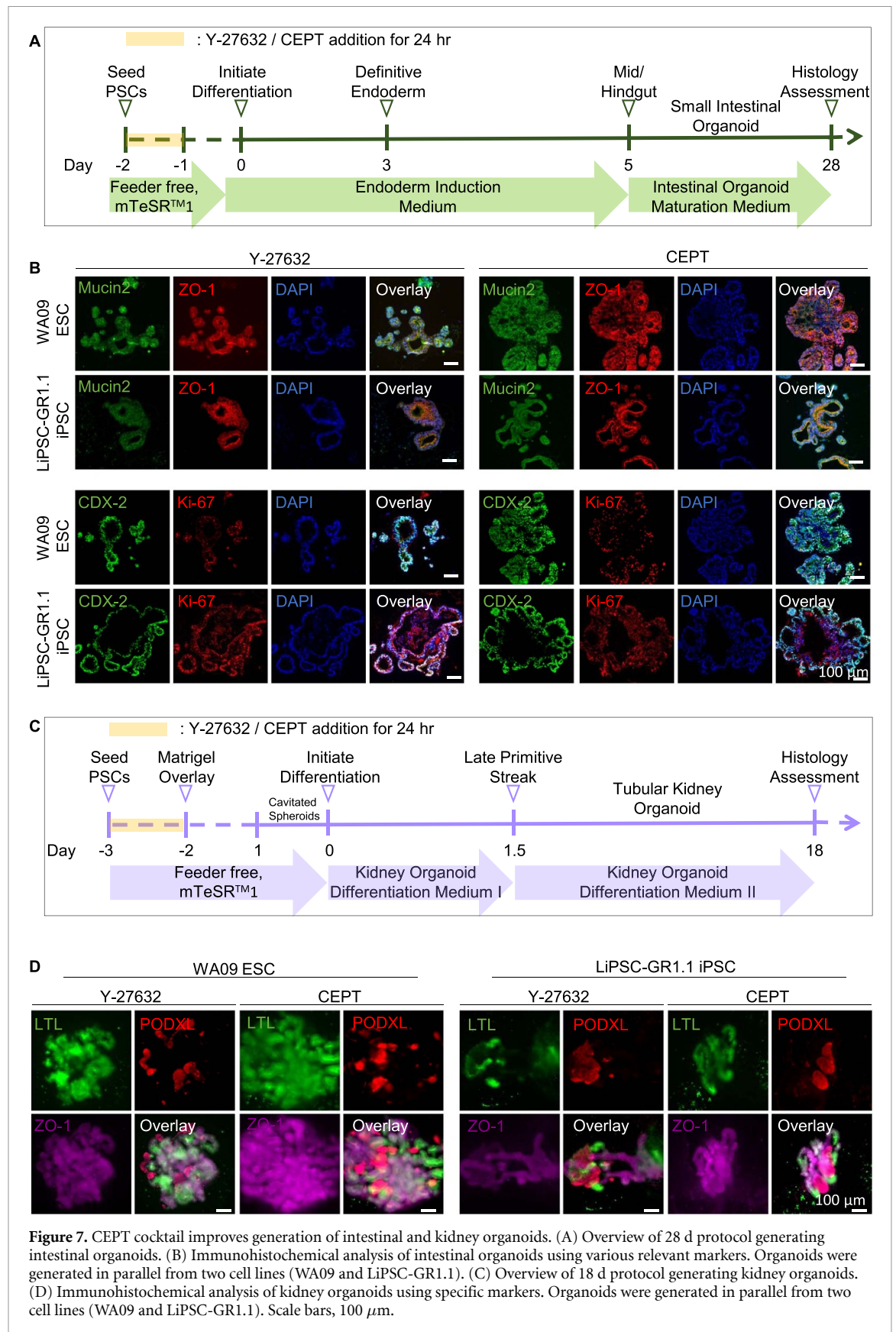


**Figure 6.** Sub-cluster analysis of WA09-derived organoids and stress markers. (A) UMAP plot for cell populations identified in organoids generated with Y-27632 or CEPT. Average expression of established cell type-specific markers. (B) Heatmap showing upregulated genes with a two-fold difference in each cluster. Each column represents a single cell clustered into unique sub-clusters based on similar gene expression profiles and each row represents an individual gene. See supplementary table 2 for the complete gene list. Red indicates maximum gene expression, while blue indicates low or no expression in log-normalized UMI counts. (C) Gene ontology terms in relation to each cell cluster are depicted in the heatmap in figure 6(B). (D) Dot plot showing expression levels for various neuronal markers and receptors in organoids generated with Y-27632 or CEPT. (E) Neuronal sub-clusters in CEPT-generated organoids indicate lower cell stress-related transcriptomics compared to those in Y-27632.

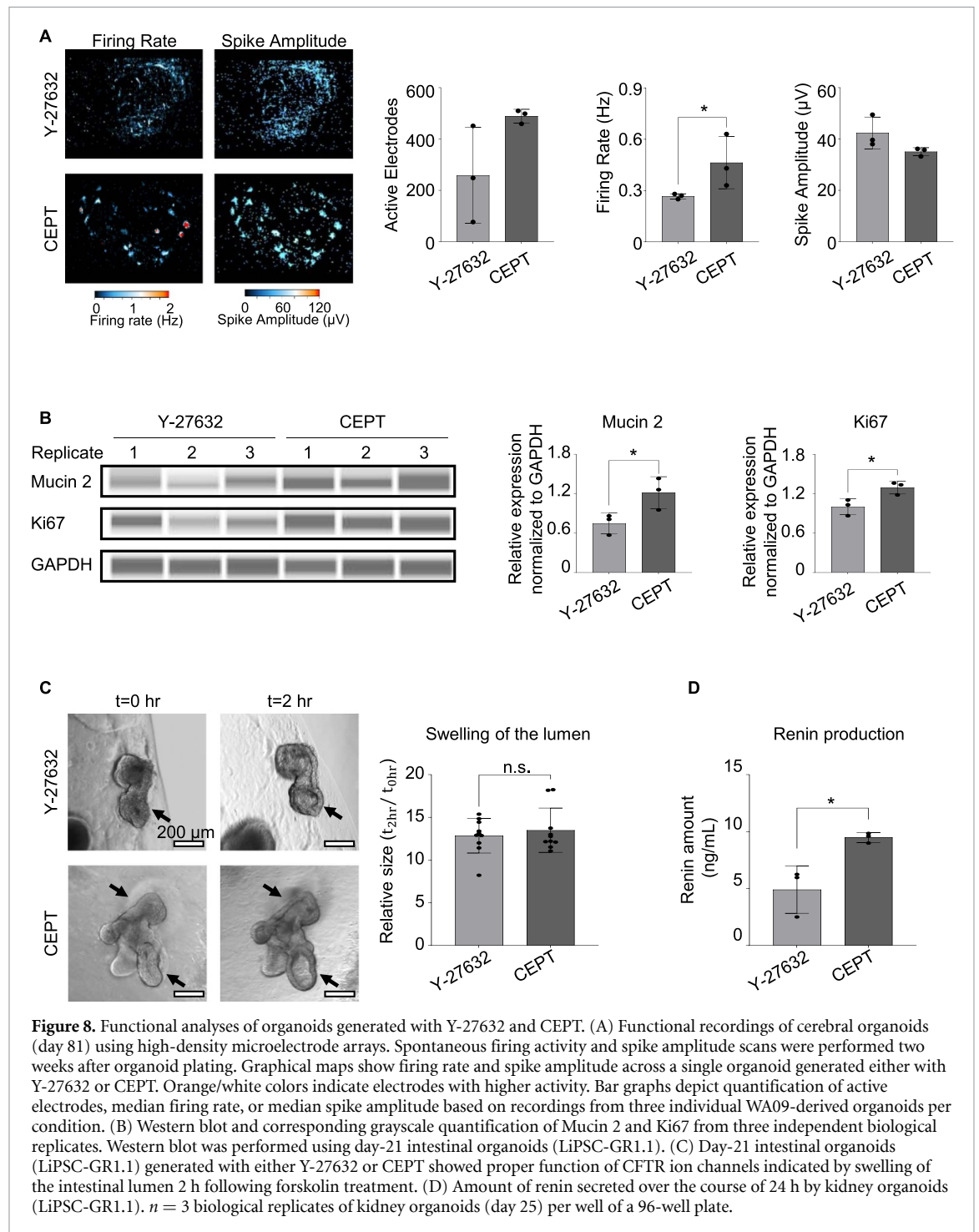
(figure 7(A)). At day 28, organoids were fixed and processed for immunohistochemical analysis using specific antibodies against mucin 2 (a marker for goblet cells), CDX2 (a marker for intestinal epithelium), ZO-1 (a marker for lumen formation), and the proliferation marker Ki67. This comparison showed that CEPT treatment generated improved

intestinal organoids with tissue-specific architecture, including polarized epithelial cells surrounding lumen-like structures (figure 7(B)). In comparison to Y-27632, CEPT treatment generated intestinal organoids that were significantly larger and displayed more complex morphologies (supplementary figure 7(A)).



Kidney organoids were generated using Y-27632 according to the manufacturer recommendation or by using CEPT for 24 h (figure 7(C)). At day 18, organoids from two different hPSC lines were

fixed and processed for whole-mount immunohistochemistry. Nephron segments were stained using proximal tubule marker lotus tetragonolobus lectin (LTL), podocyte marker PODXL (podocalyxin),



and epithelial marker (ZO-1) (figure 7(D) and supplementary figure 7(B)). Immunostainings and phase-contrast microscopy showed clear differences between organoids generated with Y-27632 or CEPT (figure 7(D), supplementary figures 7(B) and (C)). Kidney organoids generated using CEPT were significantly larger as compared to Y-27632.

### 3.8. CEPT improves organoid function

Next, we used various functional assays to determine if CEPT treatment also improves organoid function when compared to Y-27632. To measure the

function of brain organoids, spontaneous electrical activity was monitored using high-density microelectrode arrays (figure 8(A)). We observed that cerebral organoids generated with CEPT were more electrically active, as indicated by a higher number of active electrodes, and faster firing rates. However, no significant difference was detected in spike amplitudes when comparing organoids generated with Y-27632 or CEPT. For the analysis of intestinal organoids, we performed Western blots to evaluate the expression of Ki67 and Mucin 2, a gel-forming mucus protein that is secreted from goblet cells of the

intestine and functions as an important intestinal barrier (figure 8(B)) [36]. This analysis demonstrated that Ki67 and Mucin 2 expressions were higher in CEPT-generated organoids versus Y-27632 (figure 8(B)). Next, a forskolin-induced organoid swelling assay was performed to assess if intestinal organoids express functional ion channels representing the cystic fibrosis transmembrane conductance regulator (CFTR) [37, 38]. Cyclic adenosine monophosphate levels in intestinal organoids increase after stimulation with forskolin, causing opening of the CFTR channel, chloride ion transport, and swelling of the organoid lumen due to water transport by osmosis. This assay demonstrated that both CEPT- and Y-27632-generated intestinal organoids increased in size following forskolin administration, suggesting the presence of functional CFTR ion channels (figure 8(C)). To evaluate the function of the kidney organoids, the amount of renin, a key enzyme produced by kidney cells to control sodium levels and blood pressure [39], was measured at day 25 (figure 8(D)). This analysis demonstrated that CEPT-generated organoids secreted higher levels of renin when compared to Y-27632. Together, these findings indicate that organoids generated by using CEPT show improved differentiation and functional performance.

#### 4. Discussion

Cell aggregation and self-organization have been used for over a century to study the simple metazoan *Hydra* [40]. More recently, these tissue engineering methods have been employed to generate various stem cell-based 3D models such as EBs, neurospheres, assembloids, and organoids from different developmental lineages [1, 4, 15, 19, 22, 41–43]. Culturing hPSCs is particularly challenging as these cells are inherently sensitive to environmental perturbations and require special cell culture conditions, media, and reagents. The CEPT small molecule cocktail dramatically improves cell viability by preventing multiple stress mechanisms and DNA damage, that are currently underestimated in the stem cell field [9]. Here, we extended those findings and provide novel data on EB formation and four different organoid models that benefit from CEPT treatment.

While a previous study provided descriptive data on EBs and cerebral organoids [9], our current study provides an in-depth comprehensive analysis on how CEPT and its four components synergize and contribute to the generation of high-quality EBs and organoids. First, we elucidated that CEPT prevents cellular damage and ER stress and maintains the expression of cell adhesion molecules during single cell dissociation (figures 1(F) and (G)). This likely contributes to improved cell aggregation during the first 24 h, resulting not only in minimal cell loss but also healthy cells that can quickly establish cell-cell

interactions and start differentiating in a normal environment. Second, high-throughput gene expression profiling of single EBs by using RASL-Seq analysis showed that CEPT was capable of improving multi-lineage differentiation (figure 2). Third, generating organoids from three different cell lines and performing various experiments and integrated analyses of individual organoids (brain, kidney, gut), we demonstrated that CEPT treatment improved reproducibility, normal differentiation, and enhanced maturation (figures 3–7). Lastly, we performed specific assays showing that CEPT improved function across different organoid models (figure 8).

The use of self-organizing 3D models, organoids, and assembloids has become popular over the last decade. However, standardization and reproducibility remain major challenges for establishing highly robust protocols that can be utilized across laboratories. For instance, employing organoid-based disease modeling requires stringent cell culture methods and careful analyses to identify disease-specific signatures and phenotypes, which otherwise may be confounded by poor cell survival, compromised cell aggregation, and other cell culture artifacts. The challenge of experimental variability and other limitations of organoids have been described elsewhere [44].

Efforts to improve cell survival during EB and organoid formation has been addressed by others by simply increasing the concentration of the widely used Y-27632 [3, 5, 11–13]. Our data demonstrated that optimal cell survival and cell aggregation cannot be achieved by solely inhibiting ROCK kinases 1/2 either by using Y-27632 or chroman 1. Similarly, the combination of two or three factors (figures 1(B)–(G)) was less effective than the synergistic activity provided by the four-part CEPT cocktail that simultaneously targets critical mechanisms that maintain the structural and functional integrity of sensitive cells.

It was reported that organoids ectopically activate cellular stress pathways that compromise cell type specification and cortical layer formation indicated by low numbers of EOMES+ intermediate progenitors and SATB2+ upper layer neurons [33]. Interestingly, using single-cell analysis, our experiments showed that CEPT treatment can rescue this phenotype leading to increased numbers of EOMES+ progenitors and SATB2+ neurons and improved cortical layer formation (figure 5(E)). In our comparative studies we also found increased expression levels of different NMDA receptor subunits and higher expression of TET3 (methylcytosine dioxygenase 3) suggesting improved neuronal maturation due to CEPT treatment.

To fully capitalize on organoid biology and tissue engineering, new cost-efficient strategies are required for scalability encompassing scale-up and scale-out. Recent work demonstrated that CEPT can be used for robotic biomanufacturing of EBs and nocispheres

[43, 45]. Taken together, the CEPT cocktail represents a robust chemical platform promoting standardization and stress-free formation of EBs and organoids, which can be used to develop the next-generation organoid models suitable for translational applications, drug discovery, and regenerative medicine.

### Data and code availability

Bulk and single-cell RNA-Seq data generated in this study can be found in the NCBI SRA under the Bioproject PRJNA815659. Processed RASL-Seq data files can be accessed at GEO GSE198575 (raw data: PRJNA816058). The umbrella SRA Bioproject is PRJNA816454 ([www.ncbi.nlm.nih.gov/bioproject?LinkName=bioproject\\_bioproject&from\\_uid=816058](http://www.ncbi.nlm.nih.gov/bioproject?LinkName=bioproject_bioproject&from_uid=816058)). Analysis code is available at [https://github.com/cemalley/Ryu\\_cerebral\\_organoids](https://github.com/cemalley/Ryu_cerebral_organoids).

### Acknowledgments

We are grateful for the support from the Regenerative Medicine Program (RMP) of the NIH Common Fund, NIH HEAL Initiative, and in part by the intramural research program of the National Center for Advancing Translational Sciences (NCATS), NIH. The funders had no role in study design, data collection and analysis, decision to publish, or preparation of the manuscript. A S and I S are co-inventors on a U.S. Department of Health and Human Services patent application covering the CEPT cocktail and its use. Grateful acknowledgment is extended to Dr Molly E Boutin for assistance with 3D clearing for high-content 3D imaging of organoids. Figure 5(D) was created with BioRender.com.

### ORCID iDs

Seungmi Ryu  <https://orcid.org/0000-0001-8461-5878>


Claire Weber  <https://orcid.org/0000-0002-2352-8479>

Vukasin M Jovanovic  <https://orcid.org/0000-0002-0226-1998>

Jaroslav Slamecka  <https://orcid.org/0000-0003-3610-3223>

Yogita Jethmalani  <https://orcid.org/0000-0003-3422-8356>

Hannah M Baskir  <https://orcid.org/0000-0002-2914-7896>

Jason Inman  <https://orcid.org/0000-0002-8544-3286>

John Braisted  <https://orcid.org/0000-0001-8093-6463>

Anton Simeonov  <https://orcid.org/0000-0002-4523-9977>

Ty C Voss  <https://orcid.org/0009-0002-8750-2478>

Carlos A Tristan  <https://orcid.org/0000-0002-1170-6215>

Ilyas Singeç  <https://orcid.org/0000-0003-3941-1838>

### References

- [1] Eiraku M, Watanabe K, Matsuo-Takasaki M, Kawada M, Yonemura S, Matsumura M, Wataya T, Nishiyama A, Muguruma K and Sasai Y 2008 Self-organized formation of polarized cortical tissues from ESCs and its active manipulation by extrinsic signals *Cell Stem Cell* **3** 519–32
- [2] Lancaster M A and Huch M 2019 Disease modelling in human organoids *Dis. Model. Mech.* **12** 1–14
- [3] Mansour A A, Gonçalves J T, Bloyd C W, Li H, Fernandes S, Quang D, Johnston S, Parylak S L, Jin X and Gage F H 2018 An *in vivo* model of functional and vascularized human brain organoids *Nat. Biotechnol.* **36** 432–41
- [4] Sato T *et al* 2009 Single Lgr5 stem cells build crypt-villus structures *in vitro* without a mesenchymal niche *Nature* **459** 262–5
- [5] Velasco S *et al* 2019 Individual brain organoids reproducibly form cell diversity of the human cerebral cortex *Nature* **570** 523–7
- [6] Hendriks D, Clevers H and Artegiani B 2020 CRISPR-cas tools and their application in genetic engineering of human stem cells and organoids *Cell Stem Cell* **27** 705–31
- [7] Lee J *et al* 2020 Hair-bearing human skin generated entirely from pluripotent stem cells *Nature* **582** 399–404
- [8] Sloan S A, Darmanis S, Huber N, Khan T A, Birey F, Caneda C, Reimer R, Quake S R, Barres B A and Paşca S P 2017 Human astrocyte maturation captured in 3D cerebral cortical spheroids derived from pluripotent stem cells *Neuron* **95** 779–90
- [9] Chen Y *et al* 2021 A versatile polypharmacology platform promotes cytoprotection and viability of human pluripotent and differentiated cells *Nat. Methods* **18** 528–41
- [10] Ohgushi M *et al* 2010 Molecular pathway and cell state responsible for dissociation-induced apoptosis in human pluripotent stem cells *Cell Stem Cell* **7** 225–39
- [11] Watanabe K *et al* 2007 A ROCK inhibitor permits survival of dissociated human embryonic stem cells *Nat. Biotechnol.* **25** 681–6
- [12] Lancaster M A, Corsini N S, Wolfinger S, Gustafson E H, Phillips A W, Burkard T R, Otani T, Livesey F J and Knoblich J A 2017 Guided self-organization and cortical plate formation in human brain organoids *Nat. Biotechnol.* **35** 659–66
- [13] Koehler K R, Nie J, Longworth-Mills E, Liu X-P, Lee J, Holt J R and Hashino E 2017 Generation of inner ear organoids containing functional hair cells from human pluripotent stem cells *Nat. Biotechnol.* **35** 583–9
- [14] Ortmann D and Vallier L 2017 Variability of human pluripotent stem cell lines *Curr. Opin. Genet. Dev.* **46** 179–85
- [15] Keller G M 1995 *In vitro* differentiation of embryonic stem cells *Curr. Opin. Cell Biol.* **7** 862–9
- [16] Tsankov A M, Akopian V, Pop R, Chetty S, Gifford C A, Daheron L, Tsankova N M and Meissner A 2015 A qPCR scorecard quantifies the differentiation potential of human pluripotent stem cells *Nat. Biotechnol.* **33** 1182–92
- [17] Gabriel E *et al* 2021 Human brain organoids assemble functionally integrated bilateral optic vesicles *Cell Stem Cell* **28** 1740–57
- [18] Lancaster M A and Knoblich J A 2014 Generation of cerebral organoids from human pluripotent stem cells *Nat. Protocols* **9** 2329–40
- [19] Quadrato G *et al* 2017 Cell diversity and network dynamics in photosensitive human brain organoids *Nature* **545** 48–53
- [20] Saha A, Capowski E, Fernandez Zepeda M A, Nelson E C, Gamm D M and Sinha R 2022 Cone photoreceptors in human stem cell-derived retinal organoids demonstrate intrinsic light responses that mimic those of primate fovea *Cell Stem Cell* **29** 460–71

- [21] Li H, Qiu J and Fu X D 2012 RASL-seq for massively parallel and quantitative analysis of gene expression *Curr. Protocols Mol. Biol.* **4** 1–9
- [22] Lancaster M A, Renner M, Martin C-A, Wenzel D, Bicknell L S, Hurles M E, Homfray T, Penninger J M, Jackson A P and Knoblich J A 2013 Cerebral organoids model human brain development and microcephaly *Nature* **501** 373–9
- [23] Boutin M E, Voss T C, Titus S A, Cruz-Gutierrez K, Michael S and Ferrer M 2018 A high-throughput imaging and nuclear segmentation analysis protocol for cleared 3D culture models *Sci. Rep.* **8** 1–14
- [24] Scuderi S, Altobelli G G, Cimini V, Coppola G and Vaccarino F M 2021 Cell-to-cell adhesion and neurogenesis in human cortical development: a study comparing 2D monolayers with 3D organoid cultures *Stem Cell Rep.* **16** 264–80
- [25] Lachmann A, Torre D, Keenan A B, Jagodnik K M, Lee H J, Wang L, Silverstein M C and Ma'ayan A 2018 Massive mining of publicly available RNA-seq data from human and mouse *Nat. Commun.* **9** 1–10
- [26] Miller J A *et al* 2014 Transcriptional landscape of the prenatal human brain *Nature* **508** 199–206
- [27] Rowitch D H and Kriegstein A R 2010 Developmental genetics of vertebrate glial-cell specification *Nature* **468** 214–22
- [28] Trujillo C A *et al* 2019 Complex oscillatory waves emerging from cortical organoids model early human brain network development *Cell Stem Cell* **25** 558–69
- [29] Isaac J T R, Ashby M C and McBain C J 2007 The role of the GluR2 subunit in AMPA receptor function and synaptic plasticity *Neuron* **54** 859–71
- [30] Paoletti P, Bellone C and Zhou Q 2013 NMDA receptor subunit diversity: impact on receptor properties, synaptic plasticity and disease *Nat. Rev. Neurosci.* **14** 383–400
- [31] Stoyanova E, Riad M, Rao A and Heintz N 2021 5-Hydroxymethylcytosine-mediated active demethylation is required for mammalian neuronal differentiation and function *elife* **10** 1–23
- [32] Perera A *et al* 2015 TET3 is recruited by REST for context-specific hydroxymethylation and induction of gene expression *Cell Rep.* **11** 283–94
- [33] Bhaduri A *et al* 2020 Cell stress in cortical organoids impairs molecular subtype specification *Nature* **578** 142–8
- [34] Freedman B S *et al* 2015 Modelling kidney disease with CRISPR-mutant kidney organoids derived from human pluripotent epiblast spheroids *Nat. Commun.* **6** 1–13
- [35] Spence J R *et al* 2011 Directed differentiation of human pluripotent stem cells into intestinal tissue *in vitro* *Nature* **470** 105–9
- [36] Grondin J A, Kwon Y H, Far P M, Haq S and Khan W I 2020 Mucins in intestinal mucosal defense and inflammation: learning from clinical and experimental studies *Front. Immunol.* **11** 1–19
- [37] Fair K L, Colquhoun J and Hannan N R F 2018 Intestinal organoids for modelling intestinal development and disease *Phil. Trans. R. Soc. B* **373** 1–10
- [38] Dekkers J F *et al* 2013 A functional CFTR assay using primary cystic fibrosis intestinal organoids *Nat. Med.* **19** 939–45
- [39] Shankar A S *et al* 2021 Human kidney organoids produce functional renin *Kidney Int.* **99** 134–47
- [40] Layer P G, Robitzki A, Rothermel A and Willbold E 2002 Of layers and spheres: the reaggregate approach in tissue engineering *Trends Neurosci.* **25** 131–4
- [41] Reynolds B A and Weiss S 1992 Generation of neurons and astrocytes from isolated cells of the adult mammalian central nervous system *Science* **255** 1707–10
- [42] Singec I, Knoth R, Meyer R P, Maciaczyk J, Volk B, Nikkhah G, Frotscher M and Snyder E Y 2006 Defining the actual sensitivity and specificity of the neurosphere assay in stem cell biology *Nat. Methods* **3** 801–6
- [43] Tristan C A *et al* 2021 Robotic high-throughput biomanufacturing and functional differentiation of human pluripotent stem cells *Stem Cell Rep.* **16** 3076–92
- [44] Andrews M G and Kriegstein A R 2022 Challenges of organoid research *Annu. Rev. Neurosci.* **45** 23–29
- [45] Deng T *et al* 2023 Scalable generation of sensory neurons from human pluripotent stem cells *Stem Cell Rep.* **18** 1030–47